Image quality assessment for iris biometric

Kalka, Nathan, Zuo, Jinyu, Schmid, Natalia, Cukic, Bojan

Nathan D. Kalka, Jinyu Zuo, Natalia A. Schmid, Bojan Cukic, "Image quality assessment for iris biometric," Proc. SPIE 6202, Biometric Technology for Human Identification III, 62020D (17 April 2006); doi: 10.1117/12.666448

SPIE.

Event: Defense and Security Symposium, 2006, Orlando (Kissimmee), Florida, United States

Image Quality Assessment for Iris Biometric

Nathan D. Kalka, Jinyu Zuo, Natalia A. Schmid, Bojan Cukic
Lane Department of Computer Science and Electrical Engineering
West Virginia University, Morgantown, WV 26506, USA
{kalka, jinyuz, natalias, cukic}@csee.wvu.edu

ABSTRACT

Iris recognition, the ability to recognize and distinguish individuals by their iris pattern, is the most reliable biometric in terms of recognition and identification performance. However, performance of these systems is affected by poor quality imaging. In this work, we extend previous research efforts on iris quality assessment by analyzing the effect of seven quality factors: defocus blur, motion blur, off-angle, occlusion, specular reflection, lighting, and pixel-counts on the performance of traditional iris recognition system. We have concluded that defocus blur, motion blur, and off-angle are the factors that affect recognition performance the most. We further designed a fully automated iris image quality evaluation block that operates in two steps. First each factor is estimated individually, then the second step involves fusing the estimated factors by using Dempster-Shafer theory approach to evidential reasoning. The designed block is tested on two datasets, CASIA 1.0 and a dataset collected at WVU. Considerable improvement in recognition performance is demonstrated when removing poor quality images evaluated by our quality metric. The upper bound on processing complexity required to evaluate quality of a single image is $O(n^2 \log n)$, that of a 2D-Fast Fourier Transform.

Keywords: Iris image quality, iris recognition, quality factors, Dempster-Shafer theory, belief function, defocus blur, motion blur

1. INTRODUCTION

Image quality assessment plays an important role in automated biometric systems for two reasons: (1) System performance (recognition and segmentation), and (2) Interoperability. For example, low quality iris data such as in Fig. 1; result in poor recognition performance provided that traditional processing of iris images[1,2] is applied. These images have poor lighting, defocus blur, off-angle, and heavy occlusion, which have a negative impact on even the best available segmentation algorithms, also shown in Fig. 1.

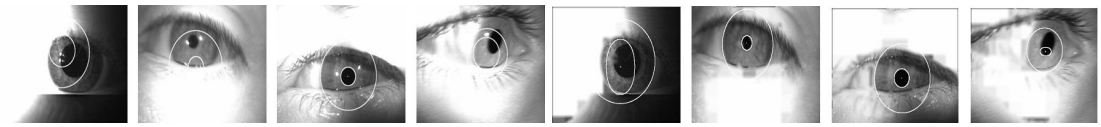

(a) Daugman's Segmentation Results (b) Wildes's Segmentation Results

Figure 1. Failed iris segmentations using our interpretation of (a) Daugman's and (b) Wildes's algorithms

It is desirable to measure the quality of data when combining different datasets to promote interoperability depending on the algorithm used.[3–5] This becomes more critical as new algorithms for biometric based recognition emerge and new acquisition systems possessing high imaging capabilities become available.

Previous work on iris image quality can be placed into two categories: local and global analysis. Zhu[6] evaluates quality by analyzing the coefficients of particular areas of iris texture by employing discrete wavelet decomposition. Chen et al.[7] classify iris quality by measuring the energy of concentric iris bands obtained from 2-D wavelets. Ma et al.[8] analyze the Fourier spectra of local iris regions to characterize defocus, motion and occlusion. Zhang[9] examines the sharpness of the region between the pupil and the iris. Daugman[2] and Kang[10] characterize quality by quantifying the energy of high spatial frequencies over the entire image region. The major drawback of most existing approaches is that evaluation of iris image quality is reduced to estimation of a single,[2,7,9] or a pair of factors,[8] such as defocus blur, motion blur, and occlusion. In addition, previous

Biometric Technology for Human Identification III, edited by Patrick J. Flynn, Sharath Pankanti,
Proc. of SPIE Vol. 6202, 62020D, (2006) · 0277-786X/06/$15 · doi: 10.1117/12.666448

literature on evaluation of iris quality involves some form of segmentation with the intent of local analysis on the iris texture.[6,7,9] Moreover, the majority of previously designed algorithms for evaluation of iris image quality require involvement of traditional segmentation methods that are iterative and thus computationally expensive.

In this paper we introduce a comprehensive approach to assess image quality from an iris biometric. We identify a broad range of factors including defocus blur, motion blur, occlusion, specular reflection, lighting, off-angle, and pixel-counts. We then analyze their individual and combined effect on traditional iris recognition systems. There are currently no iris image databases publicly available that provide enough data with the factors mentioned. Therefore using a subset of users from CASIA[11] and WVU datasets, we initially evaluate the overall affect of individual quality factors on recognition performance by synthetically degrading image quality. The intent of this analysis is to evaluate the importance of these factors as well as evaluate which factors can be reasonably quantified. Finally using intuition and knowledge gained from our synthetic research, we quantify defocus blur, motion blur, occlusion, specular reflection, lighting, off-angle, and pixel-counts and then fuse the estimated information using Dempster-Shafer theory in an effort to attain quality bounds on iris image quality. Descriptions of synthetic analysis and estimation are provided only for defocus blur, motion blur and off-angle due to lack of space. Note that in this work, we do not require iris segmentation for evaluation of global image quality and involve only a "rough segmentation" method to evaluate local iris quality. This is accomplished by image down-sampling, then employing our own interpretation of Daugman's[2] or Wildes's[1] segmentation algorithms.

The remainder of this paper is organized as follows. Section 2 describes and analyzes our synthetic studies. Section 3 describes our procedures for estimation of quality factors. Section 4 introduces information fusion framework known as Dempster-Shafer[12–15] theory. Section 5 includes results, and Section 6 concludes this work.

2. SYNTHETIC STUDIES

In our synthetic studies we use a subset of iris images from CASIA and WVU datasets (10 classes per dataset, 2 images per class) that yielded high quality images (determined by visual inspection). We synthetically degrade image quality and evaluate recognition performance. The intent of our synthetic analysis is to evaluate the importance of these factors as well as evaluate which factors can be reasonably quantified. To evaluate the influence of individual quality factors we invoke two algorithms (i) a traditional Gabor filter based iris encoding algorithm (our interpretation of Daugman's algorithm) and (ii) the global Independent Component Analysis (ICA)-based encoding method[16,17] . We intentionally use two distinct iris encoding techniques to simultaneously analyze the robustness of recognition system response on encoding techniques. The corresponding metrics that we use as measures of performance are Hamming and Euclidean distances. In this work because of the lack of space we display only results for the traditional Gabor filter-based method and present the results of analysis for three major factors in terms of performance degradation factors. Each figure demonstrating the degradation of performance will contain two plots: an error-bar plot of genuine scores and an error-bar plot of imposter scores displayed as functions of a parameter characterizing the strength of a quality factor under study. Listed below are procedures that were carried out to evaluate the quality factors.

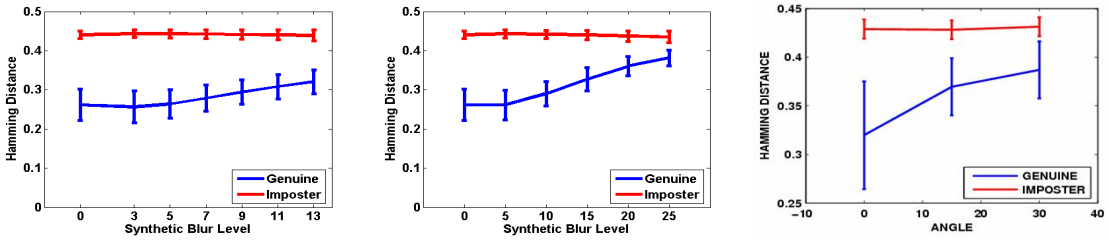

(a) Defocus Blur (b) Motion Blur (c) Off-Angle

Figure 2. Effect of Defocus, Motion, and Off-Angle on Gabor-based encoding algorithm

2.1. Defocus Blur

Defocus blur can result from many sources, but in general, defocus occurs when the focal point is outside the "depth of field" of the object to be captured. The further an object is from this depth of field the higher the degree of defocus. Depth of field is affected by aperture size, the smaller the aperture size the greater the depth of field. To simulate this factor we convolve a sequence of low-pass Gaussian filters with our iris images. As seen in Fig. 2(a), the performance degrades as blur level increases. Defocus level corresponds to the size of filter ($\sigma = 5$ for all sizes). We observed that low blur levels slightly denoise image content whereas high blur levels suppress high spatial frequency image content and hence result in the degradation of performance.

2.2. Motion Blur

Motion blur can result either from the relative motion of an object or relative motion of the camera during exposure time. In general, there are two types of motion blur, linear and non-linear. Linear motion blur can be thought of as smearing in only one direction while non-linear involves smearing in multiple directions at different strengths. We consider only linear motion blur. This factor is simulated by linearly modeling two parameters: direction of smear, denote it by Θ, and pixel-smear amount (strength). Motion strength corresponds to the length of the blur in pixels. Fig. 2(b) illustrates how increasing the motion blur strength affects the performance of encoding/recognition techniques. We observed that even small amounts of motion blur significantly degrade performance, invariant to the direction of the blur.

2.3. Off-Angle

Iris images which are not frontal view images are of special interest. For evaluating the effect of off-angle on performance, initial testing is done on thirty six iris classes from the WVU's off-angle iris image database. The database has 208 iris classes, four images per class including two from frontal views, one from 15 degree view, and one 30 degree view. The initial angle values are those assigned during the data collection. To evaluate the effect of off-angle, we train recognition systems on frontal view images and tested on off-angle images brought into frontal view by using the projective transformation. The dependence of matching score values on the angle for a Gabor based recognition system is displayed in Fig. 2(c). As the angle increases, the relative distance between the imposter and genuine score curves narrows.

3. ESTIMATION OF FACTORS

In this work, we do not require full iris segmentation for evaluation of global image quality and involve only a "rough segmentation" method to evaluate local iris quality. This is accomplished by image down-sampling, then employing our own interpretation of Daugman's[2] or Wildes's[1] segmentation algorithms. Following this, estimated segmentation parameters are further rescaled back to original image size. The local analysis is performed on the normalized iris region.

3.1. Estimation of Defocus

Defocus primarily attenuates high spatial frequencies. Due to this relationship, defocus can be assessed by measuring high frequency content in the overall image or "roughly" segmented iris region. Daugman demonstrated this in[2] by proposing an (8x8) convolution kernel and measuring the total power in the response. This 2-D spectral power is then passed through a compressive non-linearity of the form:

$$f(x) = 100 * \frac{x^2}{(x^2 + c^2)} \tag{1}$$

in order to get a normalized score between 0 and 100. Here x is the total power spectrum measured by the (8x8) convolution kernel and c is the half-power of a focus score corresponding to 50%.

This spectral measure of focus works well when iris images are canonical about the iris as in Fig. 3 (a). However, when dealing with imaging not canonical about the iris, this spectral measure of focus can be misleading as in Fig. 3 (c).

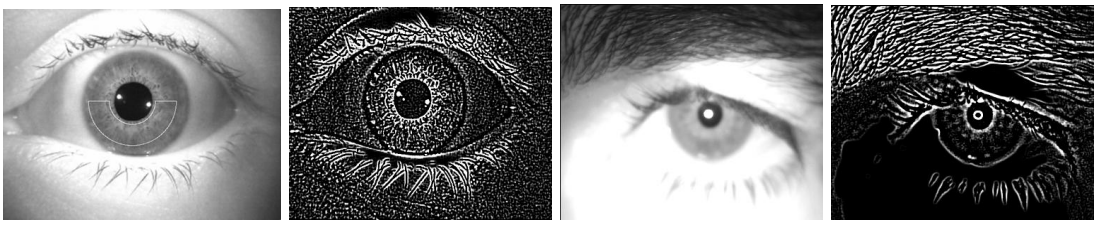

(a) Canonical (b) Filter Response (c) Non-Canonical (d) Filter Response

Figure 3. Sample images from WVU dataset and their filter responses.

Fig. 3 (b) and (d) display the responses of the band pass filtering when applied to Fig. 3 (a) and (c), respectively. Notice in Fig. 3 (b) that the iris region contains a significant amount of high spatial frequencies hence a highly focused image. In Fig. 3 (d) on the other hand, the iris region does not contain high frequency information. We conclude therefore that the iris region is defocused. However, introduction of in focus eyebrows in (d) results in a high focus global score hence the need for local focus assessment. To compensate for this we employ the same spectral measurement of focus but locally rather than globally. We also modify the compressive non-linearity to become:

$$f(x) = \frac{x^2}{(x^2 + P^2)}, \tag{2}$$

where x is the total power spectrum measured by an (8x8) convolution kernel and P is now the total power contained in the original image portion as defined by the local assessment region which is illustrated in Fig. 3 (a). This region was experimentally chosen as the upper iris region is more likely to be occluded from the upper eyelid. The notion of P was introduced such that normalization is tolerant across datasets. It was experimentally found to give good results based on CASIA & WVU datasets.

3.2. Estimation of Motion

Motion blur, as described previously, results from the relative motion between the object or camera during exposure time, which can result in linear and non-linear blur. Currently this work only includes estimation of linear motion.

Estimating linear motion blur is essentially estimating the primary direction in the image, along with the strength of this direction. To estimate the angle, we apply directional filters in Fourier space. The input image is subjected to a Fourier transform as seen in Fig. 4 (arrow A). The dot product between the transformed input image and directional masks/filters similar to those shown in Fig. 4 (arrow B) (at 36 equally spaced orientations in the range (0, 180) degrees) is performed. The total power is calculated from each of these responses. The response with most directional power gives an estimate of the angle as seen in Fig. 4 (arrow C). Let I be the image. Denote by *F(I)* the Fourier transform of I. To find the estimate of the motion blur angle, we apply directional filters of a given scale α. We denote the filter response at an orientation Θ by *H(*Θ*:*α*)*. The following equation expresses this process:

$$\hat{\Theta} = \arg \max_{\Theta \in [0:5:180]} \|F(I)H(\Theta : \alpha)\|^2 \tag{3}$$

Strength is estimated by analyzing a slice of Fourier coefficients perpendicular to the estimated angle of motion blur. Note the main "lobe" in Fig. 4 right above arrow B. The width of this main "lobe" is inversely proportional to the amount of motion blur strength. By measuring the power in the main "lobe" we can obtain an estimate of linear motion blur strength. Fig. 5 (a) is a plot of Fourier coefficients perpendicular to the estimated angle. In order to get the location of the main lobe the coefficients require smoothing. Fig. 5 (b) represents the smoothed coefficients by use of B-spline with least squares approximation. Once the coefficients are smoothed a gradient based approach is used to locate the main lobe.

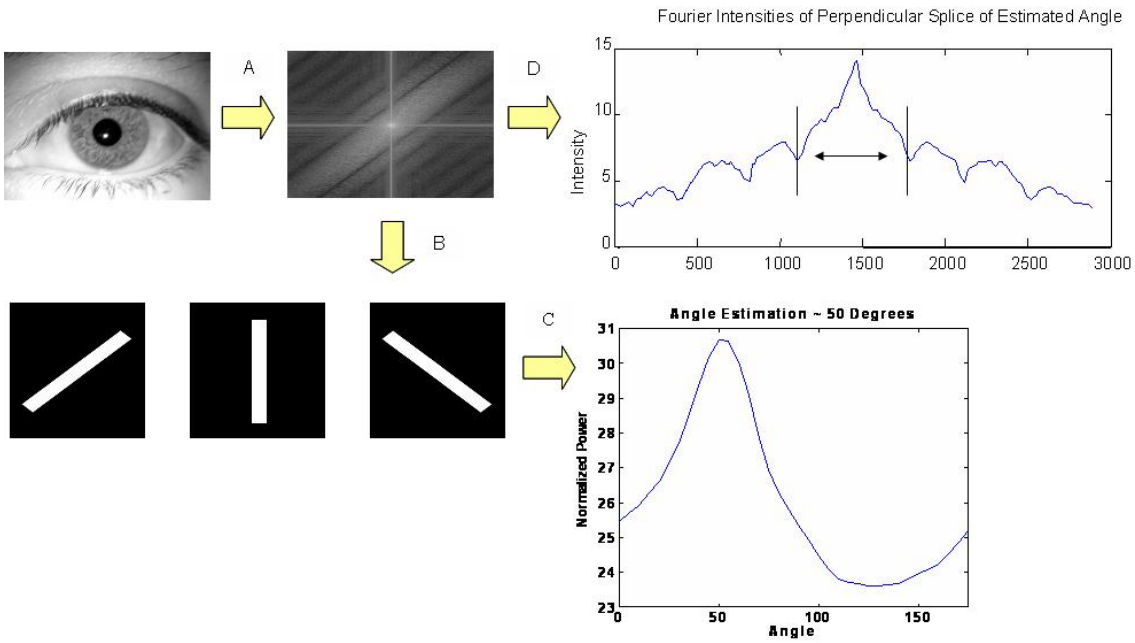

Figure 4. Motion Estimation Block Diagram

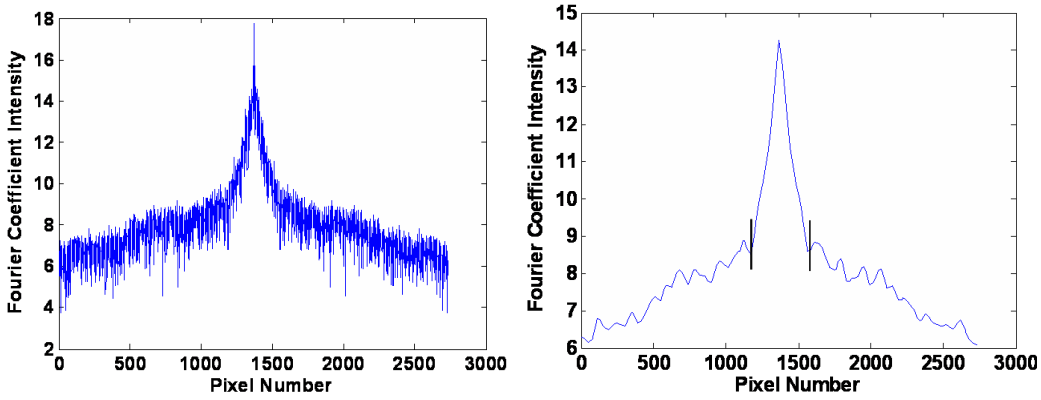

(a) Noisy Fourier Coefficients (b) Smoothed Coefficients

Figure 5. Perpendicular Fourier Coefficients

3.3. Estimation of Off-Angle

The system processes off-angle iris images by estimating the gaze direction through the application of a projective transformation to bring an iris image into a frontal view image. The general block-diagram of the estimation system is shown in Fig. 6. Below is a brief description of the estimation process. To estimate the angle of rotation we assume that a rough initial estimate of the angle is available.

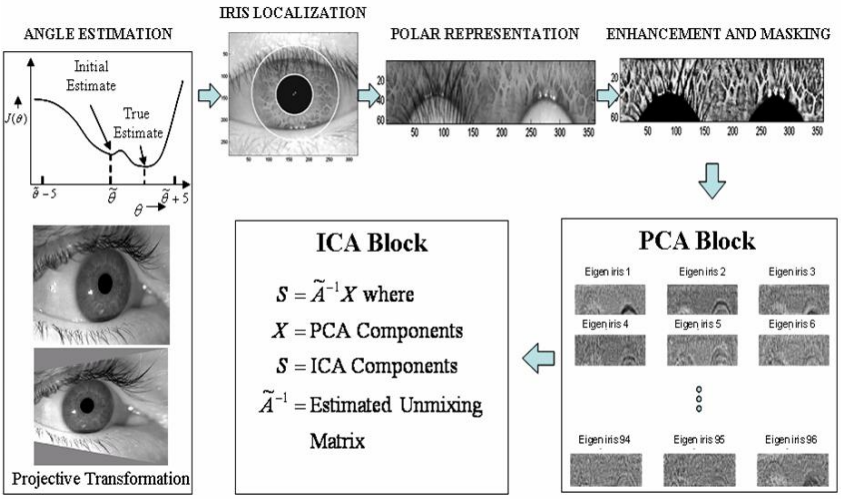

Figure 6. Off-Angle Estimation Block Diagram

The best estimate would be obtained by exhaustively searching all possible angles for roll and pitch. We use one objective function to refine the estimate: Daugman's integro-differential operator (see[2] for details of the operator) as a measure of iris circularity. We pick the estimates that maximize the value of the integro-differential operator. To be more specific, let Ψ_1 and Ψ_2 be two rotational angles and $J(\Psi_1,\Psi_2)$ be an objective function that has to be optimized. For each pair of (Ψ_1,Ψ_2) in the range $\Psi_1 \in [\Psi_{1,\min},\Psi_{1,\max}]$ and $\Psi_2 \in [\Psi_{2,\min},\Psi_{2,\max}]$, (i) the off-angle iris image is rotated by using the projective transformation and (ii) the objective function $J(\Psi_1,\Psi_1)$ is calculated. Once the angles are estimated we apply the projective transformation using the optimal angles estimated using the above procedure to rotate the off-angle image into a frontal view image. After this step, any iris recognition algorithm that operates on frontal view iris images can be applied.

4. DEMPSTER SHAFER THEORY

To generate an overall global/local quality of iris images based on the estimated individual factors, we adopt a Dempster-Shafer theory approach[12] to information fusion. This approach was proposed as a solution to a number of problems in the field of artificial intelligence, software engineering, and pattern classification.

The belief for propositions (events in Bayesian theory) start at 0, with uncertainty equal to 1. Based on incoming evidence, belief assignments are updated, hence decreasing the uncertainty. In DS theory, belief models are built on a finite boolean algebra of mutually exclusive propositions known as the frame of discernment Θ. The belief in a proposition $Bel(A)$ is a measure of certainty that A is true. Shafer gives the following expressions for assigning and measuring beliefs.

If Θ is a frame of discernment, then a function $m : 2^{\Theta} \rightarrow [0, 1]$ is called a basic probability assignment when:

1. $m(\emptyset) = 0$
2. $\sum_{A \subset \Theta} m(A) = 1.$

To measure the belief of a proposition A, one must add up the belief in all subsets B belonging to A:

$$Bel(A) = \sum_{B \subset A} m(B) \tag{4}$$

Dempsters rule of combination is used to combine beliefs over the same frame of discernment that are from distinct sources of evidence. This is measured by computing the orthogonal sum of all belief functions m which results in a new belief function based on the combined evidence.

$$m(C) = \frac{\sum\limits_{A_i \bigcap B_j = C} m_1(A_i) m_2(B_j)}{1 - \sum\limits_{A_i \bigcap B_j = \emptyset} m_1(A_i) m_2(B_j)} \tag{5}$$

Dempster's rule makes the following assumptions about evidence:

1. Independence.
2. Combination order is unimportant.

The problem with these assumptions lies in the fact that we do not have a good understanding of the dependencies between the quality factors and to assume independence between them is unreasonable (since our evidence is from the same source). In light of this, Murphy[14, 15] modified Dempster's rule such that it is suitable to use information from the same source as seen in equations (6) & (7).

$$m(C) = \frac{\sum\limits_{A_i \bigcap B_j = C} f(m_1(A_i) m_2(B_j))}{1 - \sum\limits_{A_i \bigcap B_j = \emptyset} f(m_1(A_i) m_2(B_j))} \tag{6}$$

where

$$f(m_1(A_i) m_2(B_j)) = [m_1(A_i) m_2(B_j)]^n, n \in [0, 1]. \tag{7}$$

Murphy characterizes n as a method to weight evidence. She explains that choosing $n > 0.5$ will give more weight when combining new evidence, while choosing $n < 0.5$ will give less weight when combining new evidence.[15] Other proponents of Murphy's rule characterize n as governing correlation between evidence.[13] It is explained in,[13] that choosing $n > 0.5$ assumes more independence between the evidence while choosing $n < 0.5$ assumes correlation. In light of both views choosing $n = 0.5$ is considered neutral and equal weight is applied to all evidence during integration.

4.1. Dempster Shafer Theory Applied to Quality Assessment

We adopt a frame of discernment containing two propositions which represent opposite beliefs:

1. A - Image quality is bad (Our belief that quality is bad).
2. B - Image quality is good (Our belief that quality is good).

The normalized values for each quality factor are assigned as beliefs to proposition A. Since these propositions represent opposite beliefs, the assigned belief to B is equal to the complement of the assigned belief to A. We adopt Murphy's rule of combination to combine beliefs with parameter $n = 0.5$ for all evidence. Equation (8) is a generalized expression for combining beliefs from k quality factors m_1 to m_k.

$$\hat{m}_i(A) = \frac{(\hat{m}_{i-1}(A) \cdot m_i(A))^n}{((\hat{m}_{i-1}(A) \cdot m_i(A))^n + (\hat{m}_{i-1}(B) \cdot m_i(B))^n}, i = 2, .., k \tag{8}$$

where $m_i(B) = 1 - m_i(A)$ since our propositions are complements of each other. Murphy has shown that different orderings result in different results for combined beliefs.[15] Since we have seven quality factors, that will result in 7! combinations. Our goal is to attain the orderings that result in the minimum and maximum values. These values provide valuable information about the global quality assessment of the iris image. Mladenovski[13] has proved that by sorting the beliefs in ascending order with $n = 0.5$ for all belief combinations, a maximum value can be obtained. Similarly, if sorted in descending order a minimum value can be obtained. The following section illustrates some fusion results of real data from WVU and CASIA datasets.

4.2. Evidence Fusion Examples Based on Murphy's Rule

The sample iris images in Fig. 7 are from CASIA and WVU datasets. Image (a) represents a good quality from CASIA and (c) represents a good quality image from WVU (based on visual evaluation). Images (b) and (d) represent degraded quality images which are effected by occlusion (b) and motion in (d). The estimated angle for Fig. 7 (d) is 85°.

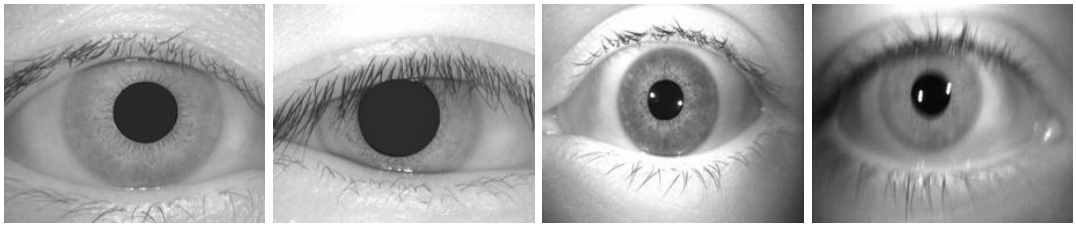

(a) CASIA (b) CASIA (c) WVU (d) WVU

Figure 7. Sample Images from CASIA and WVU datasets

Table 1 lists the estimated factors (factors are between 0 and 1, with 1 implying heavy degradation) for these images and the combined quality for them. The quality column represents the lower bound (minimum value attained from fusion of all factors) on image quality. The maximum values attained from fusion using Murphy's rule were not discriminating in terms of quality unlike the minimum values, hence we use the minimum values attained from fusion as our global quality score.

Image	Defocus	Motion	Occlusion	Specular	Lighting	Pixel Count	Quality
(a)	0.22	0.01	0.10	0.00	0.00	0.10	0.89
(b)	0.23	0.01	0.44	0.00	0.14	0.44	0.69
(c)	0.01	0.01	0.01	0.00	0.01	0.01	0.97
(d)	0.27	0.66	0.04	0.00	0.21	0.05	0.63

Table 1. Estimated Factors for images in Fig. 7

5. RESULTS

In this work we performed analysis using two iris databases, CASIA 1.0[11] and WVU database. CASIA 1.0 consists of 756 images comprising 108 classes with 7 images per class. Images were captured at a resolution of 320x280. Of the 756 CASIA images, 18 failed rough segmentation. WVU dataset consists of 2495 images taken at a resolution of 640x480. Out of the 2495 images from WVU, 370 failed rough segmentation. Any image that failed rough segmentation was discarded in order to establish a baseline for our quality metric. Table 2 list the segmentation statistics from both CASIA and WVU datasets.

Dataset	Number of Images	Failed Segmentations	Performance
CASIA	756	18	98%
WVU	2495	370	85%

Table 2. Rough Segmentation Performance

5.1. General Analysis

Fig. 8 illustrates the distribution of quality (minimum value attained from Murphy's rule with n=0.5) for (a) CASIA and (b) WVU databases. WVU suffers from many factors such as defocus, occlusion, and lighting (can also be seen in Fig. 1), which accounts for the low scoring cluster. The CASIA dataset clusters right above 0.7. Based on visual evaluation of the CASIA dataset one can conclude that the primary, if not the only factor that affects this dataset, is occlusion.

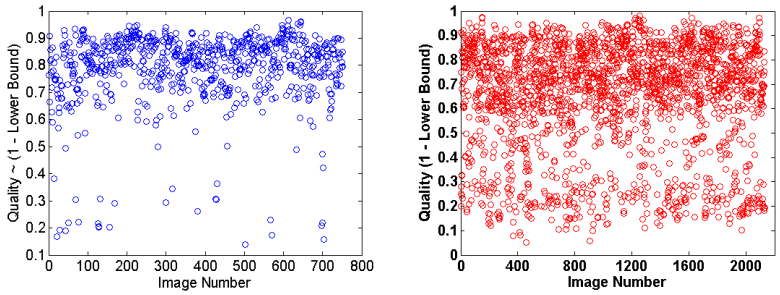

(a) CASIA (b) WVU

Figure 8. Overall Quality Scatter plots for CASIA and WVU

Table 3 summarizes mean quality scores for WVU and CASIA datasets. Based on the estimated factors for CASIA one may conclude that it is indeed primarily affected by occlusion, followed by pixel count. WVU along with CASIA is primarily affected by pixel count, followed by occlusion and lighting variation.

Dataset	Defocus	Motion	Occlusion	Specular	Lighting	Pixel Count	# of images
CASIA	0.16	0.03	0.25	0.00	0.16	0.24	738
WVU	0.13	0.05	0.30	0.01	0.30	0.31	2125

Table 3. WVU and CASIA Mean Quality Factor Scores

5.2. CASIA and WVU Performance

Performance of biometric systems is typically characterized by error rates such FAR, FRR, and EER. To evaluate the performance of our quality metric we divide CASIA and WVU datasets into three intervals based on the minimum value attained when sorting the factors in descending order. Interval one consists of the entire dataset. Interval two corresponds to those images pertaining to $quality \geq 0.75$ and interval three corresponds to those images pertaining to $quality \geq 0.85$. Equivalence classes are tallied for all the images at each interval. If no class can be established, i.e only one image from a class, then no class is established, hence it is removed.

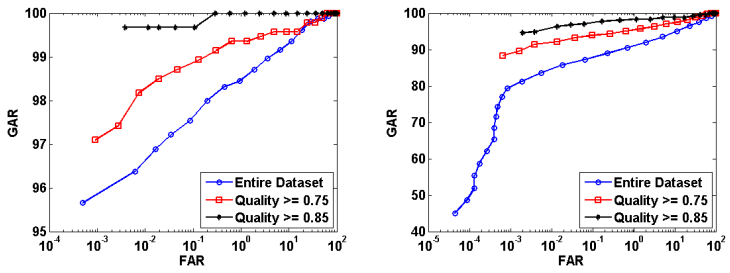

(a) CASIA Performance (b) WVU Performance

Figure 9. Verification Performance Prediction

Fig. 9 characterizes the performance at each interval. Based on the statistics in Table 4 we notice a performance increasing trend: as quality of the data increases so does performance. Table 4 lists EER, d', and mean quality values for each interval along with the number of images pertaining to each interval. The entire CASIA dataset (except for those images that failed rough segmentation) performs well, in general. However, by using our quality metric we are able to select images which can achieve the desired level of performance, with the last interval attaining an EER of 0.11 and d' of 3.13.

Interval	EER (%)	d'	Mean Quality	Image Count
All	1.30	2.63	0.79	738
Quality $\geq$ 0.75	0.63	2.79	0.85	556
Quality $\geq$ 0.85	0.11	3.13	0.89	273

Table 4. CASIA Results

Interval	EER (%)	d'	Mean Quality	Image Count
All	5.07	2.53	0.65	2125
Quality $\geq$ 0.75	3.20	2.96	0.84	841
Quality $\geq$ 0.85	1.17	3.53	0.89	393

Table 5. WVU Results

With respect to the WVU results in Fig. 9 (b) and Table 5, we again see a performance increasing trend. The last interval achieves an EER of 1.17 and d' of 3.53 which are comparable to what was achieved for CASIA.

6. CONCLUSIONS

In this work quality factors for an iris recognition biometric were identified and their individual influence on performance was studied. Since there are no public databases that exhibit the quality factors under study, we took a subset of good quality images from CASIA and WVU datasets and synthetically degraded image quality. From these studies we concluded that defocus blur, motion blur, and off-angle significantly degrade performance more than other factors.

Estimation procedures for defocus, motion blur, off-angle, occlusion, specular reflection, lighting, pixel counts were then carried out. Estimated quality scores are then fused by use of Dempster-Shafer theory in order to attain confidence bounds on image quality. We characterized quality for CASIA and WVU datasets. We noticed that CASIA dataset contains higher quality data than WVU. We also demonstrated that our quality metric can predict performance for CASIA and WVU datasets with improvements in both EER and d' as quality increases. The main limitation with this approach is requirement of "rough" segmentation. Failed localization/segmentation will result in inaccurate quality scores. Future work includes designing better estimation techniques for the described factors along with exploring the correlation between different factors.

REFERENCES

1. R. Wildes, "Iris recognition: An emerging biometric technology," *Proceedings of the IEEE* **85**, pp. 1348 – 1363, September 1997.
2. J. Daugman, "How iris recognition works," *IEEE Trans. on Circuits and Systems for Video Technology* **14**, pp. 21–30, January 2004.
3. E. Tabassi, C. L. Wilson, and C. I. Watson, "Fingerprint image quality," Tech. Rep. NISTIR 7151, NIST, 100 Bureau Drive, Stop 8940, Gaithersburg, MD 20899, August 2004.
4. M. Yao, S. Pankanti, N. Haas, N. Ratha, and R. Bolle, "Quantifying quality: A case study in fingerprints," *Proc. of IEEE Conference on Automatic Identification Advanced Technologies (AutoID)* , pp. 126–131, March 2002.
5. Z. Wang, A. Bovik, and L. Lu, "Why is image quality assessment so difficult," *Proc. of 2002 IEEE International Conference on Acoustics, Speech, and Signal Processing (ICASSP 2002)* , pp. 3313–3316, May 2002.
6. X. Zhu, Y. Liu, X. Ming, and Q. Cui, "A quality evaluation method of iris images sequence based on wavelet coefficients in 'region of interest'," *Proc. of the 4th Int'l Conf. on Computer and Information Technology* , pp. 24–27, September 2004.
7. Y. Chen, S. Dass, and A. Jain, "Localized iris quality using 2-D wavelets," *International Conference on Biometrics* , pp. 373–381, 2006. Hong Kong, China.
8. L. Ma, T. Tan, Y. Wang, and D. Zhang, "Personal identification based on iris texture analysis," *IEEE Trans. on Pattern Analysis and Machine Intelligence* **25**, pp. 1519–1533, December 2003.
9. G. Zhang and M. Salganicoff, "Method of measuring the focus of close-up image of eyes," Tech. Rep. 5953440, United States Patent, 1999.
10. B. Kang and K. Park, "A study on iris image restoration," *Proc. Audio and Video-Based Biometric Person Authentication* **3546**, pp. 31–40, July 2005.
11. "CASIA iris image database (ver 1.0)," *http://www.sinobiometric.com/casiairis.html* .
12. G. Shafer, *A Mathematical Theory of Evidence*, Princeton University Press, 1976.
13. M. Mladenovski, "Information fusion schemes for real time risk assessment in adaptive control systems," Master's thesis, West Virginia University, 2004.
14. R. Murphy, "Adaptive rule of combinations for observations over time," *Fusion and Integration for Intelligent Systems* , pp. 125 – 131, December 1996.
15. R. Murphy, "Dempster-shafer theory for sensor fusion in autonomous mobile robots," *IEEE Trans. On Robotics and Automation* **14**, pp. 197–206, April 1998.
16. V. Dorairaj, N. Schmid, and G. Fahmy, "Performance evaluation of non-ideal iris based recognition system implementing global ICA encoding," *Proc. of the IEEE International Conference on Image Processing (ICIP),* **3**, pp. 285–288, 2005.
17. V. Dorairaj, N. Schmid, and G. Fahmy, "Performance evaluation of iris based recognition system implementing PCA and ICA techniques," *Proc. of the SPIE 2005 Symp. on Defense and Security* , pp. 51–58, March 2005.